# Thermal Imaging of Quenched Microstructural Evolution in Steel Alloys

by
Nicole Zacharia

Submitted to the Department of Materials Science and Engineering
in partial fulfillment of the requirements for the degree of

Bachelor of Science in Materials Science and Engineering

at the
MASSACHUSETTS INSTITUTE OF TECHNOLOGY

June 2001

©2001 Nicole Zacharia
All rights reserved

The author hereby grants to MIT permission to reproduce and to distribute pubicly paper and electronic copies of this thesis document in whole or in part

The author hereby grants to MIT permission to reproduce and to distribute publicly paper and electronic copies of this thesis document in whole or in part in any medium now known or hereafter created.

Signature redacted

Author.....
Department of Materials Science and Engineering
May 25, 2001

Signature redacted

Certified by.....
Douglas Matson
Department Lecturer

Signature redacted

Accepted by.....
Ronald M. Latanision
Chairman, Department Committee on Undergraduate Theses

MASSACHUSETTS INSTITUTE OF TECHNOLOGY
AUG 2 1 2018
LIBRARIES
ARCHIVES

# Thermal Imaging of Quenched Microstructural Evolution in Steel Alloys

by

Nicole Zacharia

Submitted to the Department of Materials Science and Engineering
on May 25, 2001, in partial fulfillment of the
requirements for the degree of
Bachelor of Science in Materials Science and Engineering

## Abstract

A method was devised for quenching undercooled samples of Fe-12Cr-16Ni. The samples were levitated in a magnetic field as a way of containerless processing. They were dropped onto a nucleation trigger and then into a quenching bath. This process was successful in producing quenched samples, but the layer of In-Ga wetting their surface showed problematic in the analysis of the samples. Data shows that double recalescence was observed in a few cases. SEM proved inconclusive and was not sensitive enough to detect the small chemical variations expected in the dendrites. Also, across the entirety of the sample there was no significant partitioning of Cr or Ni.

Thesis Supervisor: Douglas Matson
Title: Department Lecturer

# Acknowledgements

The author would like to express her most sincere gratitude to Dr. Douglas Matson, for all of his advice, supervision, and understanding throught the course of this project. Additional thanks go to Professor Flemmings for making this project possible. Of course thanks to Joan Kertz, Lori Kensel, and Jim Yurko for being helpful group members in many ways. Don Galler and Neil Jenkins for their help with SEM imagining, and Cemal Akcaba for help with formatting this document.

# Contents

Abstract 3

Acknowledgements 4

List of Figures 7

List of Tables 9

1 Introduction 11

2 Project Objectives 15

3 Experimental 17

4 Results 21

5 Process modelling 33

6 Discussion 37

7 Conclusions 39

7.1 Processing . . . . . 39

7.2 Solidification . . . . . 40

# List of Figures


1-1 Growth rate as a function of undercooling. The solid symbols are for primary recalescence growth, and the open symbols for secondary recalescence growth. 13

2-1 Delay time as a weak function of undercooling. . . . . 16

3-1 Levitation chamber and coil. . . . . 18

3-2 The quenching bath with trigger. . . . . 20

4-1 Video imagery of sample 1. . . . . 22

4-2 Sample 1 Pyrometry Data . . . . . 23

4-3 Video imagery of sample 2. . . . . 24

4-4 Sample 2 Pyrometry Data . . . . . 25

4-5 Video imagery of sample 3. . . . . 26

4-6 Heat cycle of sample 3. . . . . 27

4-7 Light microscope picture of Sample 1. . . . . 28

4-8 Dendrites of Sample 1 . . . . . 29

4-9 Line scan across Sample 1 . . . . . 30

4-10 Concentration map of Sample 1 . . . . . 31

# List of Tables

5.1 Time for solid phase to grow. . . . . 35
5.2 Distance from trigger to quench bath. . . . . 35

# Chapter 1

# Introduction

In order to understand the non-equilibrium solidification process in undercooled metals, a few concepts such as undercooling, recalescence, solidification path, and $T_o$ must be introduced. Undercooling is a non-equilibrium state in which a substance (in this case a molten metal) has been cooled to below the melting temperature while still retaining it's liquid state. Once nucleation of the solid does occur, there will be a release of heat (from the latent heat of fusion) from the solid into the liquid, which is known as recalescence. The negative temperature gradient, which is caused by the recalescence, destabilizes the interface between undercooled liquid and a mixture of solid and liquid near the melting point, and a front propagates in the form of free dendritic growth of an array of dendrites. The larger the degree of undercooling, the higher the fraction of solid that forms during recalescence. The solidification path is the way the composition of the liquid and solid phase compositions change throughout solidification. The last key term is $T_o$, which is the temperature at which the free energy of the solid and liquid are the same. This then is the critical temperature for partitionless solidification where the liquid and solid have the same composition during rapid solidification[5].

It is well established that processing conditions such as undercooling have a very strong

influence on the selection between the metastable bcc-ferrite (delta) and the stable fcc-austenite (gamma) phase in Fe-Ni as well as Fe-Ni-Cr alloys. Following this primary recalescence when the ferrite forms is a second, slower recalescence characterized by the growth of the equilibrium phase[1]. Before the solidification is complete, much of the metastable structure formed during primary recalescence is changed by Ostwald ripening or coarsening, partial remelting, and decomposition.

For the alloy used in this study the $T_o$ above which bcc will not be able to nucleate directly from the melt is an undercooling of fifty degrees [2]. At these low undercoolings the metal is near enough to equilibrium conditions that the fcc phase energetically is favored to nucleate first, and its growth will dominate the solidification process. However, when both phases are able to nucleate directly from the melt, bcc is preferred due to surface energy considerations. Figure 1-1 shows the dendritic growth rate for bcc and fcc phases as a function of undercooling. It should be observed that growth velocity of the fcc phase during secondary recalescence is relatively independent of undercooling rate, and the reason for this is that once primary recalescence has occured, the melt is brought up to nearly the same temperature, regardless of initial undercooling[3]. Also, three zones can be identified in the figure. The first zone is above $T_o$, for which only fcc can nucleate directly. Then the second zone is from approximately undercoolings of 50° to 150°, where either phase might nucleate first, and then the third region of deeper undercoolings, where only the bcc phase will begin to nucleate.

In samples of Fe-Ni alloys solute-rich inversely cored structures are seen, and the explanation for this is remelting and coarsening during solidification. The solidification path consists of diffusionless rapid solidification, then a rise in temperature due to recalescence, and finally a decrease in temperature as equilibrium cooling takes place.

Rapid solidification comes up in industry when in places like strip casting or spray casting, when small amounts of metal are quickly cooled. The different phases have different properties, and one or other might be preferable for certain applications. If the process was

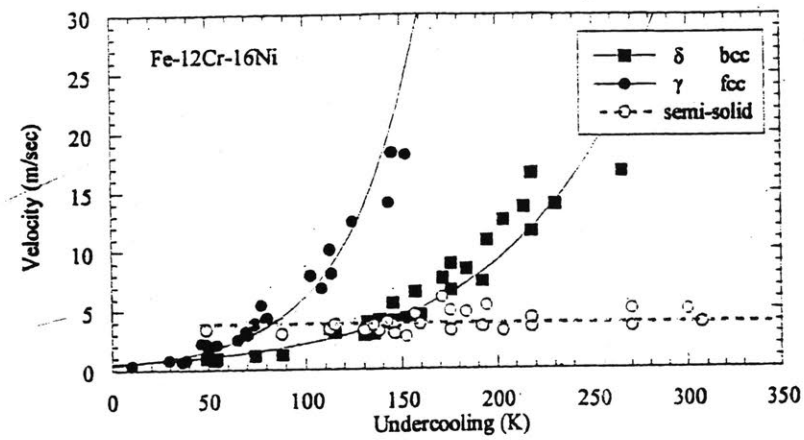


Figure 1-1: Growth rate as a function of undercooling. The solid symbols are for primary recalescence growth, and the open symbols for secondary recalescence growth.

better understood, it might even be possible to control the microstructure when casting.

# Chapter 2

# Project Objectives

The basic objective of this project is to obtain data verifying the current theories about the solidification path of Fe-Ni-Cr. To do this, quenched samples of Fe-12Ni-16Cr which had been undercooled to various temperatures will be obtained. Observation of the video data from each quench, as well as metallographic analysis of the samples well provide the desired information.

Figure 2-1 shows the correspondance of undercooling to delay time between recalescence events. It can easily be seen that there are two distinct behaviors on the graph; at low undercoolings, near $T_o$, and at high degrees of undercooling [4]. The delay time reaches a plateau as the undercooling reaches 100°K and more.

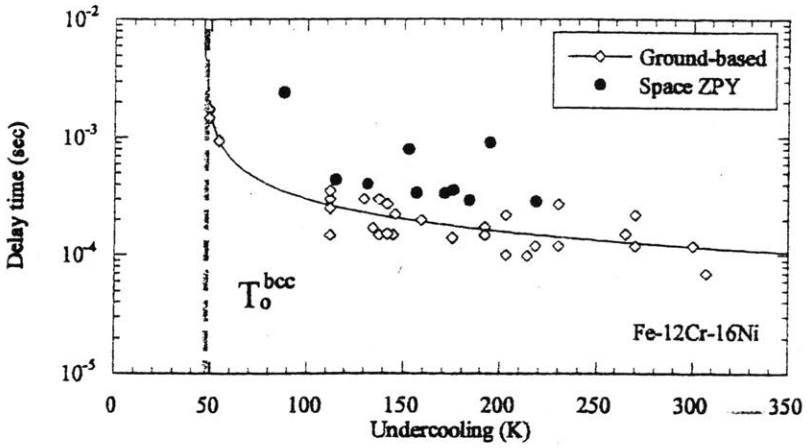


Figure 2-1: Delay time as a weak function of undercooling.

# Chapter 3

# Experimental

This project specifically investigates the properties of Fe-12Cr-16Ni alloy. One gram samples of the steel alloy were made from high purity steel, nickel, and chromium. Each metal was weighed out separately, with an error of 0.00003 g. Each metal was cut with a diamond saw, or in the case of nickel wire cut with specially reserved wire cutters, and then filed down to appropriate size with a file reserved specifically for that element in order to maintain purity. The three pieces were then alloyed together by levitating the iron in the coil until it melts, then sequentially dropping it on the chrome and then the nickel. The sample was held at a melt for 15-20 seconds in order to ensure uniformity of the sample. Eighteen such samples were prepared.

The coil can be seen in figure 3-1 as well as the levitation chamber used in the experiments. It consists of a chamber with a copper coil through which current is run to inductively heat and levitate the sample. Underneath the coil is a carousel on which there are sample holders. It is from here that the samples are lifted into the coil during the experiment. On one side of the chamber there is an opening where a pyrometer is placed to monitor the temperature, and the cover of the chamber is plexiglass to allow viewing of the solidification process.

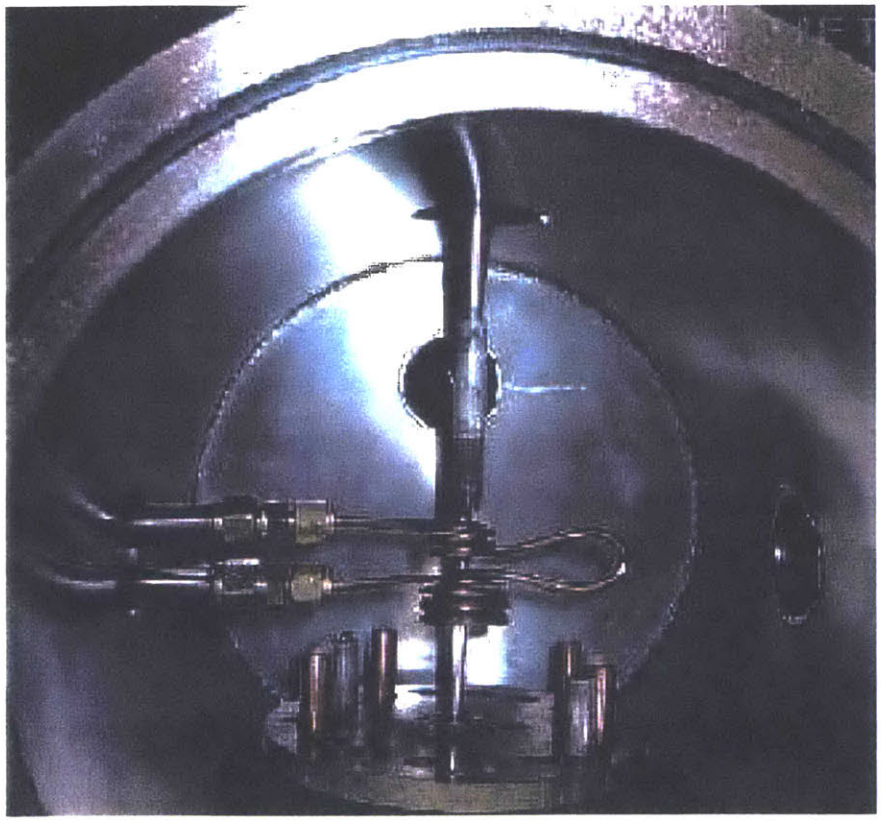

Figure 3-1: Levitation chamber and coil.

Prior to the experiment the chamber is evacuated using two vacuum pumps and purged with Ar-10% H and He-5% H. To run the experiment, the sample is lifted with the holder into the coil and a magnetic field applied. As soon as the sample begins to levitate, the sample holder is lowered from the coil. A pyrometer monitors the sample's temperature. Ar is released into the chamber until the sample becomes too hot. The Ar stream is then shut off and a He stream begins. Since He has better thermal conductivity it cools the sample. Once the desired degree of undercooling is achieved, the field is shut off, and the sample drops into a quenching bath of In-Ga. Before hitting the quenching bath, solidification is triggered by allowing the sample to touch an Fe wire, to nucleate bcc formation. This way, the exact spot where nucleation began is known. A high speed digital camera films at a frame rate of 40,500 fps films the drop to directly observe the progression of solidification. After the experiment the sample is pulled out of the bath, and the trigger is either cleaned or replaced. A schematic of this setup can be seen in figure 3-2.

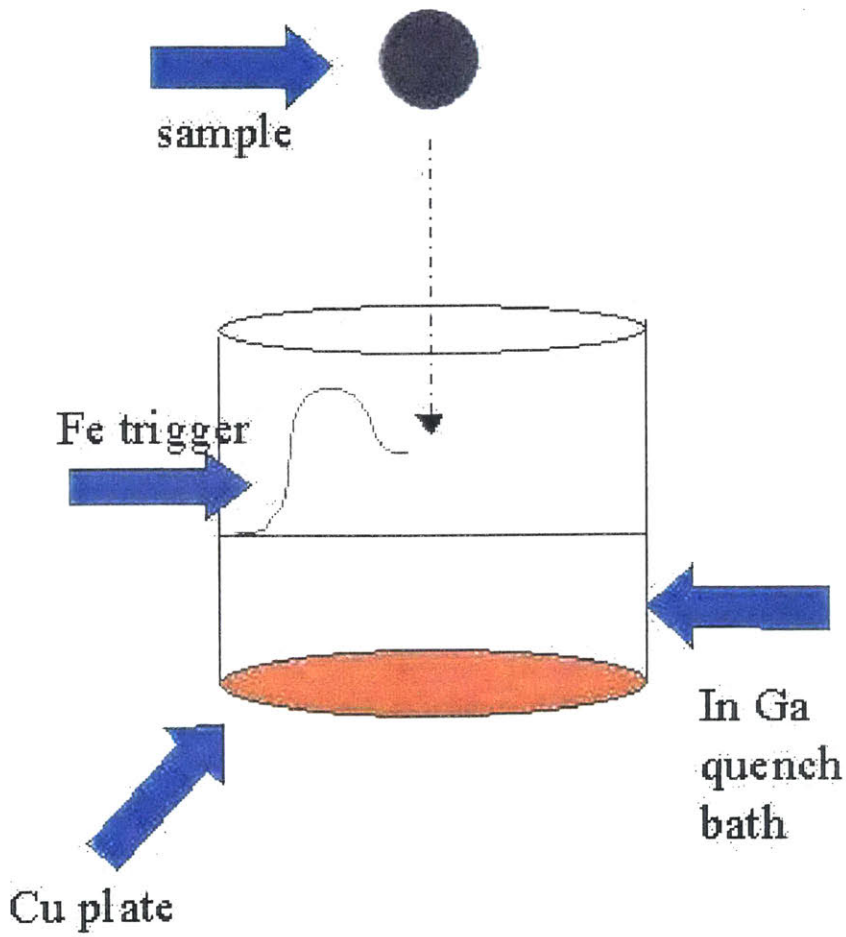


Figure 3-2: The quenching bath with trigger.

# Chapter 4

# Results

Of the 18 samples prepared, 2 were sacrificed to test the quenching technique, and another dozen were tested. Of these dozen, one sample worked but there was no video or pyrometric data, two more samples worked, and a fourth hit the trigger, but double recalescence had occured prior to triggering.

Figure 4-1 shows the the video imagery for a sample which was undercooled approximately 50°. At the end of the first row of pictures, the sample is triggered and can be seen to become lighter. This is because as the liquid solidifies heat is released. At the end of the second row a second bright front starts to move through the sample. This is the double recalescence event. Chart 4-2 shows the heating cycle which sample 1 underwent before being quenched.

Figure 4-3 shows the video imagery of sample 2, which can be seen to also undergo a double recalescence. Chart 4-4 shows the heating cycle.

Figure 4-5 shows the sample which had already double recalesced before being triggered. It can clearly be seen to approach the trigger at the end of the second row, beginning of the third row, and only one heat front is seen to propagate through the sample. Chart 4-6 shows the heating cycle for sample 3.

After being quenched, the samples were mounted in epoxy and polished. They were

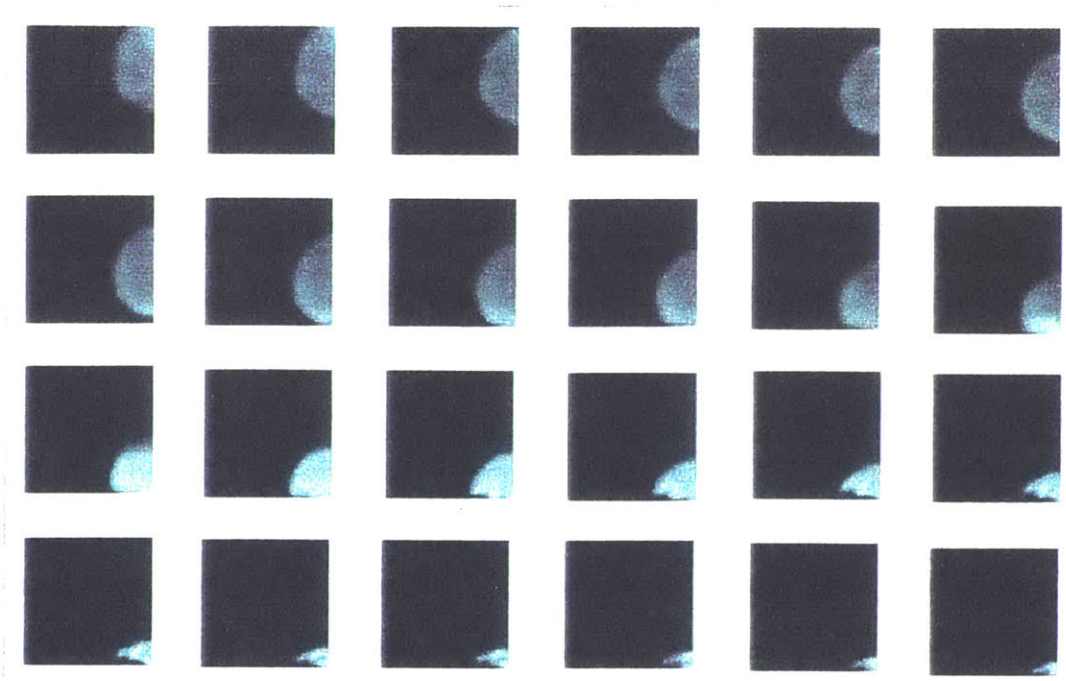

Figure 4-1: Video imagery of sample 1.

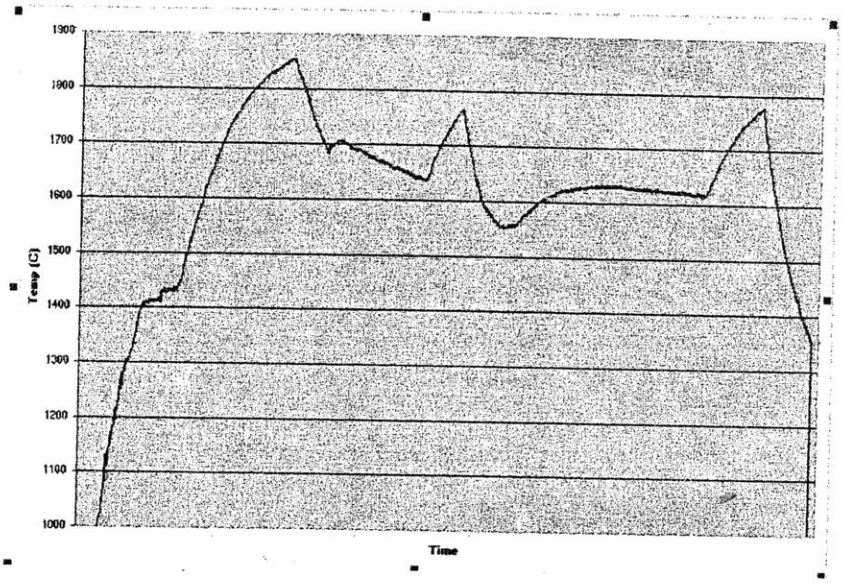


Figure 4-2: Sample 1 Pyrometry Data

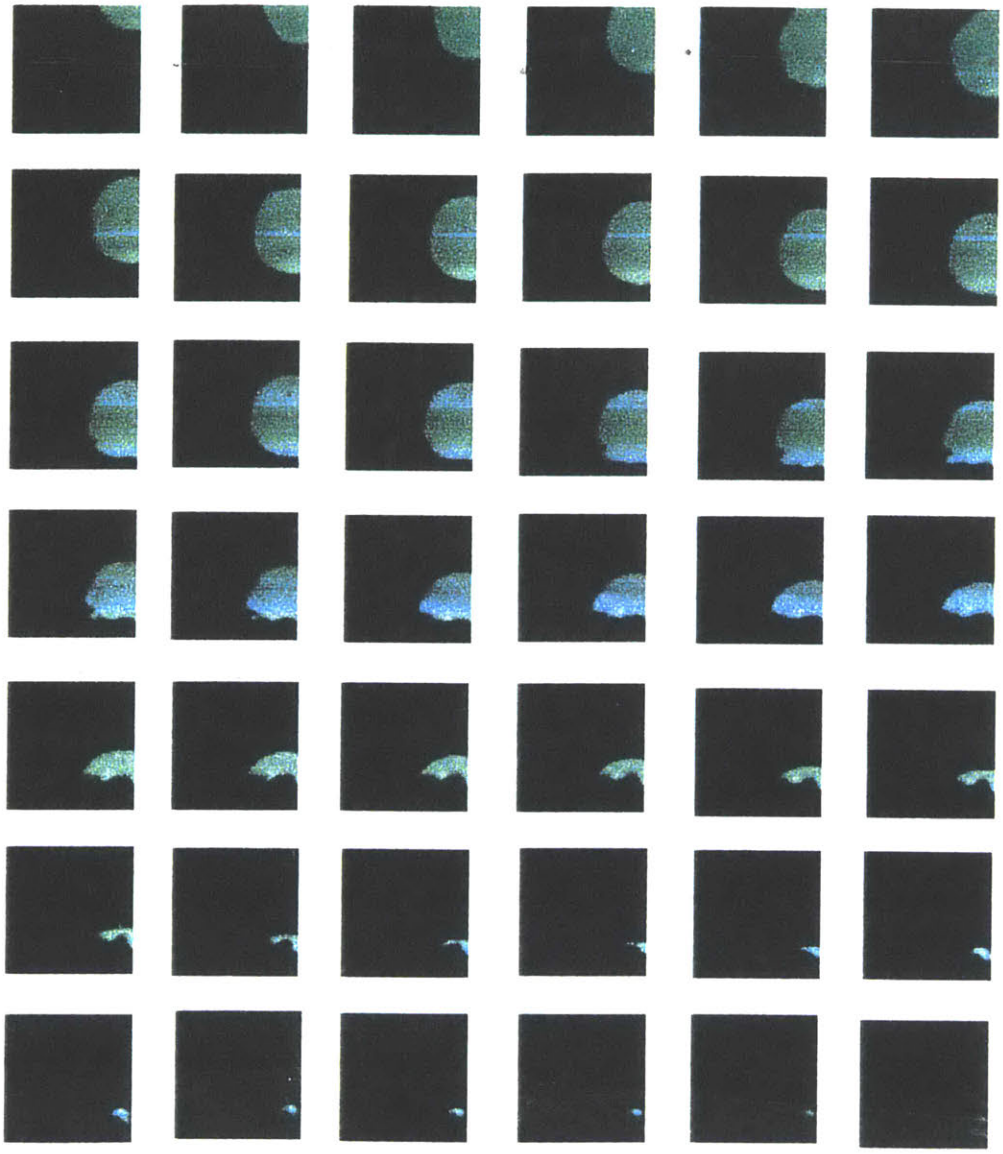

Figure 4-3: Video imagery of sample 2.

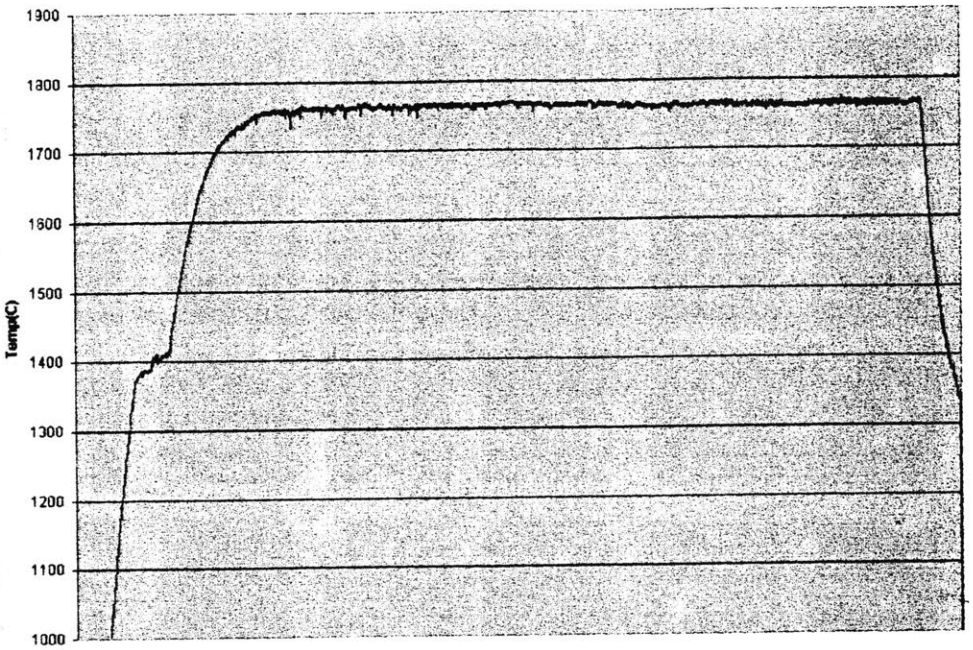


Figure 4-4: Sample 2 Pyrometry Data

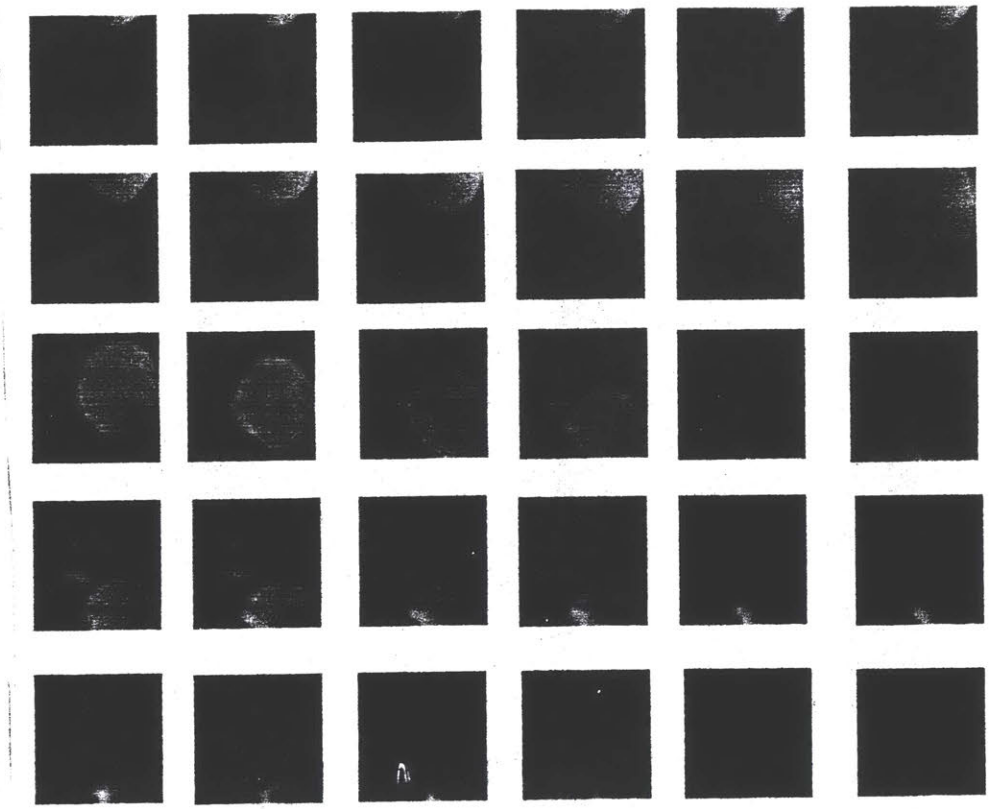

Figure 4-5: Video imagery of sample 3.

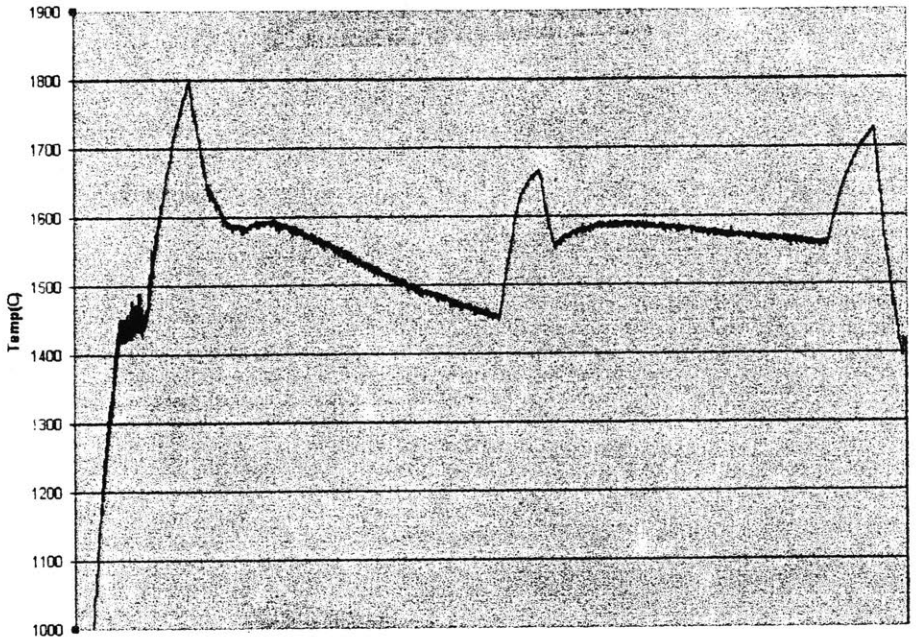


Figure 4-6: Heat cycle of sample 3.

ground with various sizes of sandpaper, They were examined optically and under SEM.

The samples were first etched with Kalling's reagent, a $CuCl_2$ based etchant. While this stained the samples, it did not reveal the dendrites and under SEM nothing was visible. Figure 4-7 shows sample 1 after being etched in an electrolytic bath of aqueous solution, 10% $H_2SO_4$. Figure 4-8 shows dendrites viewed under SEM.

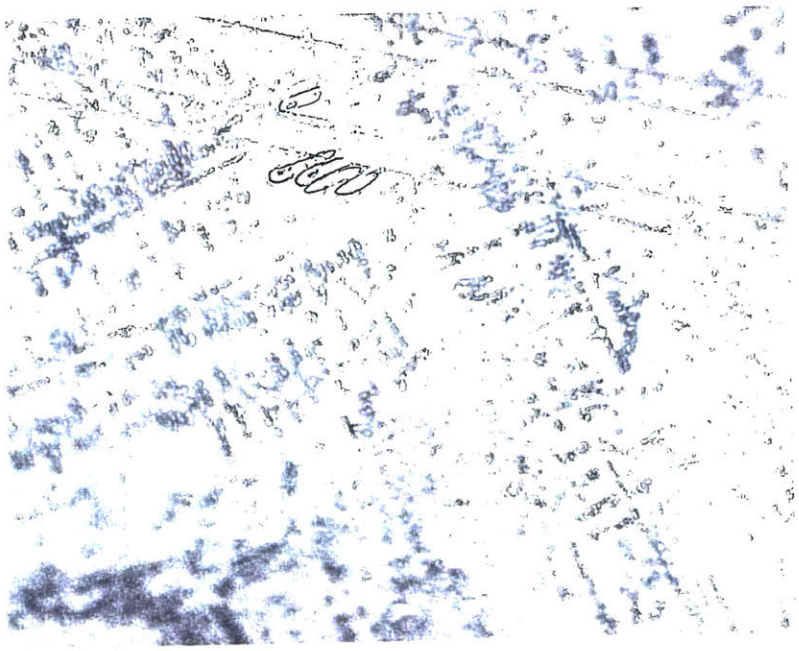

Figure 4-7: Light microscope picture of Sample 1.

Several line scans were taken by SEM of sample 1. One such scan is shown in figure 4-9; this is a scan across the entire sample. Since the dendrites are on the order of 15 $\mu$ in length, a scan a smaller feature was also taken. Figure 4-10 shows the concentration maps of Fe, Cr, and Ni across 50 $\mu$ of the sample.

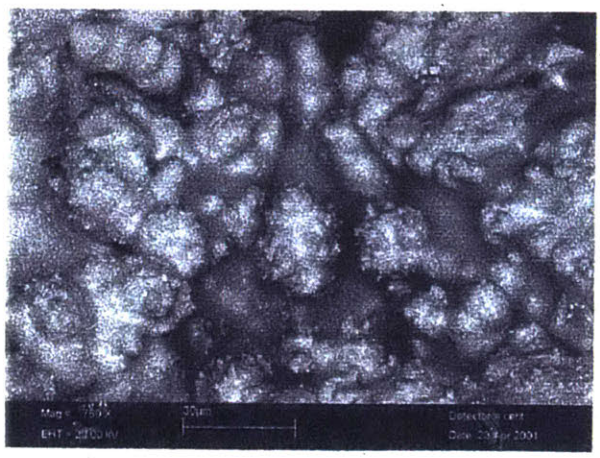

Figure 4-8: Dendrites of Sample 1

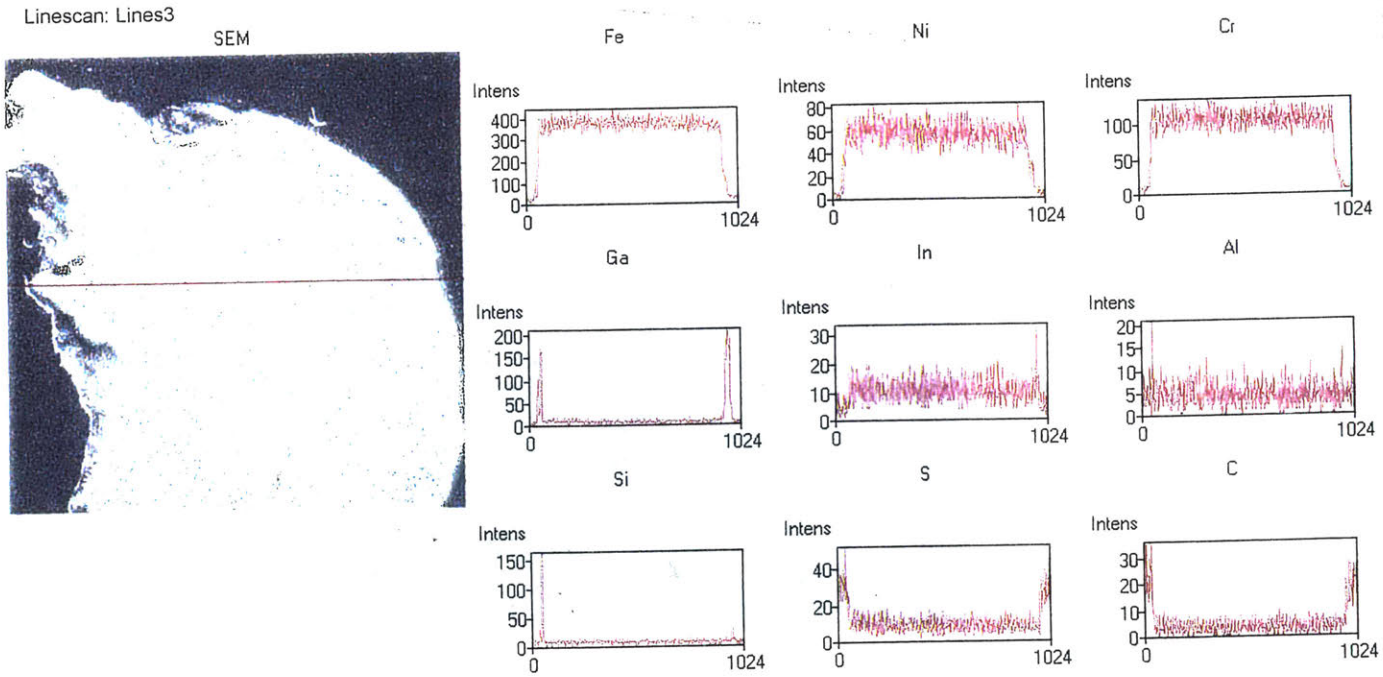


Figure 4-9: Line scan across Sample 1

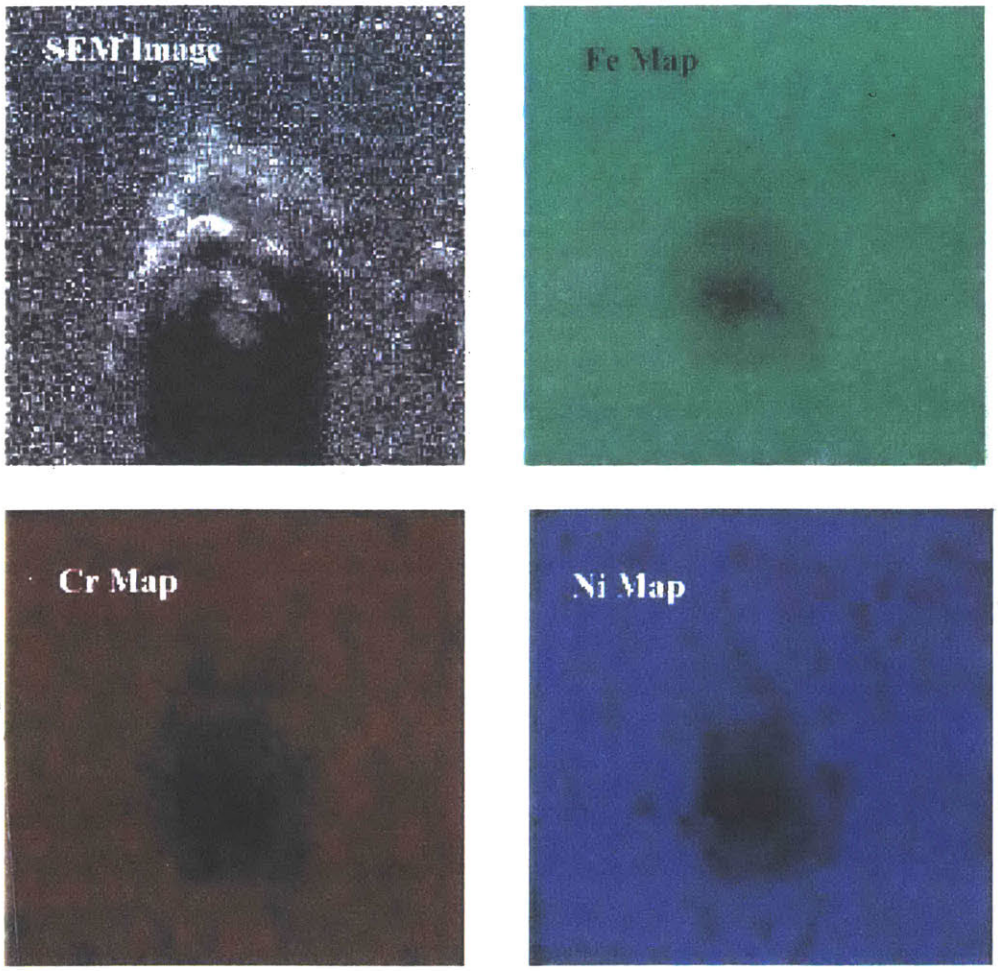


Figure 4-10: Concentration map of Sample 1

# Chapter 5

# Process modelling

A number of calculations were performed in designing the experiment to show that the experiment actually happened as intended.

To show that the degree of undercooling obtained in the coil is the same as the actual degree of undercooling upon impact, an estimate of the sample's cooling while falling from the coil to the bath was calculated uding the Ranz-Marshal equation. A steel sample with density ($\rho$) of 7800 kg/m$^3$ and diameter (D) of 1 cm at 1673°K falling at 1 m/s was assumed. The gas assumed was He at 300 °K, because the actual atmosphere would have a mix of H, Ar, and He, and He has the best thermal properties. $C_p$ was taken as 1000 J/kg°K.

film temperature, $T_f = (1673 + 300)/2 = 986.5$

for He at $T_f, \nu = 806 * 10^{-6} m^2 s^{-1}, Pr = 0.654, k = 351 * 10^{-3} W/m^\circ K$

for steel, $\epsilon = 0.3$

$Re = \frac{DV}{\nu} = \frac{(1*10^{-2}m)(1ms^{-1})}{806*10^{-6}m^2s^{-1}} = 12\ .4$

Ranz-Marshall, $Nu = \frac{h_c D}{k} = 2 + 0.6Re^{\frac{1}{2}} * Pr^{\frac{1}{3}} \ = 3.83$

$h_c = \frac{3.83*k}{D} = 134.6$

$h_r = \epsilon \cdot \frac{\sigma*[T_1^4 - T_2^4]}{(T_1 - T_2)} = 59.3$

$h_t = h_c + h_r = 193.9$

$$q = h \cdot \Delta T = 193.9 * (1673 - 300) = 2.66 * 10^5$$
$$Q = q \cdot A = m \cdot C_p(\frac{dT}{dt})$$
$$\frac{A}{m} = \frac{4\pi R^2}{\frac{4}{3}\pi R^3 \rho} = \frac{6}{D\rho} = 0.\ 077$$
$$C_p \cdot (\frac{dT}{dt}) = 20496$$
$$\frac{dT}{dt} = 20.5°K/s$$

The sample will fall about 5 cm, at the assumed speed of 1m/s, which makes for a cooling of about 1°, which for our purposes is negligible.

To estimate the amount of In-Ga quench bath, it was estimated that a sample at 1808° would be quenching to 300°K. Again, $\rho$ (Fe) = 7.86 g/cc and $C_p = 41.8\frac{J}{molK}$. The bath is 25% In by weight or 16.8 mol %, $\rho(In) = 7.31g/cc$, $\rho(Ga) = 5.907g\ /cc$, and the heat capacities are $C_{In} = 30.29 - (1.38 * 10^{-3}) \cdot T$ and $C_{Ga} = 26.36 + \frac{1.26*10^5}{T^2}$ in $\frac{J}{molK}$.

$$Q = mC_p\Delta T$$
$$Q = 1ccFe, \frac{7.86g}{55.84g/mol} \cdot 41.8[1808 - 473] = 7854.8$$
$$7854.8 = m \cdot \int C_p\, dT$$
$$= m \cdot \int_{T=300}^{473} 0.168(30.29 - (1.38 * 10^{-3}) \cdot T) + 0.833(26.\ 36 + \frac{1.26*10^5}{T^2})\, dT$$
$$7854.8 = m(12519.27 - 7743.25)$$
$$m = 1.64mol$$

This corresponds to 127 g of bath, which is 20.7 cc. The vessel containing the bath was chosen to be able to hold this amount and have walls tall enough to catch possible splashing. A copper plate was put into the vessel to prevent the glass from breaking due to thermal shock when the sample hits the bottom.

The other calculation which needed to be made was how high above the bath the trigger needed to be placed. The values for growth velocity and delay time are taken from graphs

1-1 and 2-1 respectively. The goal is to allow enough time for bcc growth on the sample's surface to be more than the fcc growth. Table 5.1 shows how long it takes for samples of different undercoolings to allow both phases to grow, including the delay time. Table 5.2 shows how far above the bath's surface the trigger must be. The total time of drop includes the time needed for the sample to fall from the coil to the trigger.

Table 5.1: Time for solid phase to grow.

| undercooling (°) | time for 4mm bcc growth | time fo r 2mm fcc growth | growth time + delay time |
|---|---|---|---|
| 50 | 0.0027s | 0.001s | 0.0037s |
| 100 | 0.002s | 0.00036s | 0.00036s |
| 120 | 0.0013s | 0.00021s | 0.000485s |
| 150 | 0.001s | 0.000093s | 0.00034s |

Table 5.2: Distance from trigger to quench bath.

| undercooling | total drop time | trigger distance (mm) |
|---|---|---|
| 50 | 0.0052s | 3.8 |
| 100 | 0.00236s | 1.7 |
| 120 | 0.00179 | 1.3 |
| 150 | 0.00134 | 0.95 |

It can be seen that for the trigger should be placed only milimeters from the bath's surface. This is important because if the sample was allowed longer to solidify, the fcc growth would entirely overtake the bcc growth.

# Chapter 6

# Discussion

The pyrometric data shows that in most cases only low undercooling (on the order of 50°). This degree of undercooling is approaching the critical temperature necessary for a double recalescence event to occur, so based on this alone it is uncertain whether or not double recalescence took place. Sample two was witnessed to flash before being dropped into the quench bath, so it that case there was certainly no double recalescence event.

The video data seems to show a double recalescence event for both samples 1 and 2. Two separate heat fronts seem to propagate through the sample. Only in sample 2 it is not entirely clear whether the second front started in the same place where the metastable phase was triggered.

Etching with the Kalling's reagent seemed to stain the samples without revealing information about the microstructure. Switching to $H_2SO_4$ in an electrolytic bath worked better, revealing finger like structures with dark centers. These dark centers should be areas of higher nickel concentration.

SEM data, however, proved inconclusive. The edges of the sample, around where growth was triggered was coated with the In-Ga, and the SEM had great difficulty picking up anything else. The wetting of the sample by the quench bath proved to be a great difficulty.

The most interesting data should be in these areas. Further into the sample, the effects of coarsening should be seen. Also, the quenching was not as instantaneous inside the sample as near the surface.

The line scans through the sample are too noisy to show whether there are local differences in chemical composition. The scan across the entire sample shows that while there might be some variance the average composition is consistent. This is not entirely expected, because as the metal solidifies in bcc phase, it rejects chromium into the environment. The molten metal will then have a higher concentration of Cr and a concentration gradient should develop. However, here we see no significant change across the sample's surface. The concentration maps of the smaller region show that Fe concentration is fairly consistent, and that Ni and Cr do seem to vary. In this scan points were taken at about every 0.25 $\mu$. The compositions do seem to vary from point to point, but in a way which suggests random scattering as opposed to partitioning of elements in one region or another.

# Chapter 7

# Conclusions

## 7.1 Processing

A new method for quenching undercooled samples was developped. Models were developed which seem to show that degree of undercooling can be accurately predicted and that it is possibly to nucleate bcc growth soon enough before quenching so that fcc growth has not entirely replaced the bcc growth.

The actual experimental set up worked well in that the trigger was hit nearly every time and the copper plate at the bottom of the bath worked as hoped. The video camera was used successfully to record the trials. However, the high degree of wetting of In-Ga onto the samples proved to be a great difficulty. The most interesting microstructures should occur right at the surface of the sample, and more specifically right where the trigger hit the sample. Unfortunately the layer of In-Ga prohibited this structure from being seen.

An etching process using an electrolytic bath of $H_2SO_4$ was developed. This etching technique nicely exposed the microstructure of the samples under light microscopy, but unfortunately did not show anything under the SEM. For SEM work another process should be developed.

## 7.2 Solidification

The data shows that low degrees of undercooling were reached, and several times a double recalescence was triggered. A dendritic microstructure was seen under light microscopy. SEM data, however, was not conclusive enough to prove whether or not coring took place in the dendrites. The differences in concentration across a dendrite should be on the order of only a few percent, and SEM simply cannot give this resolution. A microprobe should be used to gather this data. One piece of information gained from the SEM scans is that partitioning of the Cr and Ni throughout the sample as a whole is not significant, as might be expected.

# Bibliography


[1] T Koseki, MC Flemmings, *Metallurgical and Materials Transactions A*, 1996, vol. 27A, p. 3226-3240.

[2] J Kertz, MIT master's thesis with Prof. Flemmings, 2001.

[3] C. Bui, MIT master's thesis with Prof. Flemmings, 1998.

[4] L. Kensel, MIT master's thesis with Prof. Flemmings, in progress.

[5] Fisher, Kurz, *Fundamentals of Solidification*, Trans Tech Publications LTD, 1998